Chinese Journal of Aeronautics, (2025), 38(7): 103554

Chinese Society of Aeronautics and Astronautics
& Beihang University

Chinese Journal of Aeronautics

cja@buaa.edu.cn
www.sciencedirect.com

FULL LENGTH ARTICLE

Improved surface integrity in Inconel 718 using small diameter hammer peening tools

Aitor MADARIAGA [a,*], Gorka ORTIZ-DE-ZARATE [b], Pedro José ARRAZOLA [b]

[a] Department of Materials, University of Manchester, Manchester M13 9PL, United Kingdom
[b] Mechanical and Industrial Production Department, Faculty of Engineering, Mondragon Unibertsitatea, Arrasate 20500, Spain

Received 13 May 2024; revised 26 June 2024; accepted 31 July 2024
Available online 25 April 2025

KEYWORDS

In-situ tests;
Machine hammer peening;
Nickel-based alloy;
Residual stresses;
Surface integrity;
X-ray diffraction

Abstract Machine hammer peening (MHP) is an emergent treatment that induces high compressive residual stresses (RS) which can enhance the in-service performance of components. This paper studies the use of small diameter MHP tools to improve the Surface Integrity (SI) of the nickel-based alloy Inconel 718 used in critical aero-engine components. Complementarily, the relaxation of RS is analyzed by *in-situ* annealing tests at in-service temperature combined with X-ray diffraction measurement. For this purpose, age hardened Inconel 718 discs were turned as reference condition, and then a pneumatic MHP tool was used under different conditions: two tool diameters (4 mm and 12 mm), feed rates (2.5 m/min and 5.0 m/min) and stepover distances (0.07 mm and 0.35 mm). Subsequently, surface topography characterization, RS measurements, nanoindentation tests, and microstructural observations were conducted. The *in-situ* annealing tests were done in the X-ray diffractometer at 550 °C for exposure periods from 0 to 20 h. The results demonstrate that 4 mm diameter tools generate smooth surfaces and induce significant compressive RS within a 0.5 mm thick layer. Residual stresses are relaxed, but they remain compressive even after a long thermal exposure. The microstructure of the surface layer (< 10–15 μm) was affected by the preceding turning operation, but importantly, MHP did not induce additional damage.

1. Introduction

Nickel-based alloys have extraordinary mechanical strength and corrosion resistance at elevated temperatures, and they have become a unique and most popular alternative of key aerospace components.[1] They are widely selected to manufacture aero-engine critical components subjected to high thermo-mechanical in-service loads, such as turbine discs. Nevertheless, these alloys are difficult-to-cut due to their properties and behavior during the cutting process:[2] low thermal

* Corresponding author.
E-mail address: aitor.madariaga@manchester.ac.uk (A. MADARIAGA).

Peer review under responsibility of Editorial Committee of CJA

ELSEVIER Production and hosting by Elsevier

https://doi.org/10.1016/j.cja.2025.103554

conductivity, prone to work-hardening, retention of high strength levels at high temperatures, reactivity with cutting tool materials, tendency to form built-up-edge and presence of abrasive carbides in their microstructure. If proper machining process window is not selected, the Surface Integrity (SI) of machined nickel-based alloy parts can be affected irreversibly (tensile surface residual stresses, rough surface topography, increased hardness and/or microstructural anomalies), and thus dramatically impact their final performance.[3] For this reason, stringent controls are carried out on the manufacturing of critical components to ensure performance and safety throughout their service life.[4]

In this context, significant research studies have analyzed the SI after machining aero-engine alloys over the last decade as summarized in recent literature reviews.[5,6] These studies have allowed understanding the effect of machining parameters on SI of nickel-based alloys. However, surface mechanical treatments are usually applied after the machining process to reduce the risk of fatigue failure caused by thermomechanical in-service loads.[7] The preferred surface treatments are Shot-Peening (SP) and Laser Shock Peening (LSP), which induce compressive Residual Stresses (RS) that retard crack initiation and propagation. Klotz et al.[8] compared the SI and fatigue performance of polished, as-machined and three SP conditions. Shot-peening induced –1 000 MPa compressive RS and about 10% increase in hardness near the surface, and stabilizing at 100–200 μm depth depending on parameters. However, roughness increased from Rt = 7.15 μm in the as-machined condition, to Rt = 8.65–11.90 μm when using low intensity SP, and to Rt = 25.38 μm when applying the highest intensity SP. Importantly, they found that High Cycle Fatigue (HCF) behavior was dominated by RS and Low Cycle Fatigue (LCF) by surface roughness. Consequently, high intensity SP reduced the LCF life with respect to the as-machined condition. Kattoura et al.[9] found that appropriate selection of LSP parameters can generate thicker RS compressive layers (about 400 μm) in nickel-based alloys than SP, with slightly lower surface RS (–800 MPa) leading to an improved fatigue strength. Nevertheless, LSP increased surface roughness from Ra = 0.02 μm (polished samples) to Ra = 2.08 μm, which could have limited the positive effect of the compressive RS. For this reason, a surface polishing process is necessary after SP or LSP to gain the required surface finishing,[7] but unfortunately the later steps will produce unacceptable tensile RS.

Machine Hammer Peening (MHP) is an emerging mechanical surface treatment and can be an alternative of SP and LSP. MHP can provide a wide range of material property improvements in the surface layer:[10] material hardening, generation of compressive RS, surface smoothening or recrystallization refinement. These improved properties increase the fatigue strength, corrosion resistance or tribological properties of the treated component. For this reason, MHP is gaining more relevance in industrial applications for improving the performance of structural parts or smoothing dies.[11] MHP is based on the oscillating motion of an axially guided hammering tool, which impacts the target surface. The actuator can be pneumatic, ultrasonic, piezoelectric or electromagnetic.[10] This actuator is attached to a machine tool or a robot, and thus allows performing a controlled surface modification.[12] This is one of the key advantages with respect to SP or similar peening processes, because they cannot guarantee that the impact intensity is uniform across the treated area. MHP is also a cleaner process compared to SP since no dust it is generated, and the quantity of needed lubrication is minimal.[10] Furthermore, it does not need additional medium on the material of the surface contact, in contrast to other treatments such as LSP.

Many researchers have studied the application of MHP to improve the fatigue performance of welding zones or smoothening of dies used in automotive industry,[10] but very few works have analyzed the effect of MHP on the SI and in-service performance of nickel-based alloys used in the aeronautic and energy sectors. In a pioneering work, Chen et al.[13] studied the effect of MHP on the SI and corrosion resistance of an oil-grade Inconel 718 in annealed state. They hammer peened the milled surface with a 12 mm diameter indenter (type of actuator undefined), using a hammering frequency of 140 Hz and two feed rates (2 m/min and 4 m/min). The hardness of the treated surface increased by 50–100 HV with respect to the milled surface, and by 200–250 HV with respect to the bulk material. It also induced compressive surface RS (–600 MPa when using 2 m/min and –730 MPa when using 4 m/min), a smooth surface (Ra < 0.5 μm) and formation of ultrafine grains beneath the surface. This improved SI led to a significant increase in corrosion resistance. In a complementary work,[14] they applied a double aging treatment (760 °C for 4–5 h followed by 650 °C for 4–5 h) to the milled and hammer peened surfaces. The hardness of the bulk material increased by 260 HV and the hardness of the hammer peened surfaces by 160 HV, but compressive RS were almost fully relaxed, and the corrosion resistance of hammer peened specimens decreased after aging. Although they demonstrated the capability of MHP to improve the SI of Inconel 718 in annealed state, the mechanical properties differed from the solution treated and aged hardened Inconel 718 used in the aeronautic sector and results are not extrapolatable. Later, Trauth et al.[15] employed a piezoelectric hammer peening actuator with a 12 mm diameter tool to treat Inconel 718 surfaces cut by Wire Electro Discharge Machining (W-EDM) at 100 Hz hammering frequency, 0.9 mm stroke, 0.1 mm pitch and 6 m/min feed rate. These conditions were selected based on a previous work of the research group conducted on steel X155CrMoV12 with 58 HRC hardness,[16] which is significantly harder than the selected Inconel 718 (about 40–43 HRC). MHP significantly decreased the roughness of the EDM finished samples from Ra = 1.10 μm to Ra = 0.14 μm, increased the surface hardness up to 46 HRC, and induced high compressive RS within 400 μm depth, being these more compressive perpendicular to the feed direction (up to –1 150 MPa at the surface). Subsequent fatigue characterization demonstrated that the fatigue strength of hammer peened specimens was 1.4 higher that W-EDMed specimens as consequence of the improved SI. Sarasua Miranda et al.[17] tested different MHP conditions using a pneumatic actuator with a 20 mm diameter tool at 250 Hz frequency to treat an age hardened Inconel 718 specimen cut by W-EDM. The best set of conditions (5 m/min feed rate, 1 mm initial offset) induced very high surface compressive RS (–1 000 MPa in the feed and –1 750 MPa perpendicular direction respectively), but selected conditionswere not able to reduce the roughness Ra below 12 μm. More recently, Jin et al.[7] adopted an optimized set of parameters (impact frequency of 100 Hz, stroke of 1.5 mm, stepover distance of 0.1 mm, indentation distance of 0.1 mm and feed rate of 6 m/min), to treat commercially available Inconel 718 (initial hardness of 286 HV). The tool diameter and type of actuator

were not defined. They demonstrated that MHP treatment smoothens the surface ($Ra < 0.3$ μm) and produces a compressive RS layer (thickness > 1 mm) with maximum compressive stress up to –1 430 MPa, as well as an increase of about 50% in surface hardness. Nevertheless, they did not define the diameter of the tool, and the hardness of the raw material was significantly lower than the age hardened Inconel 718 used in aero-engine critical components.

Aero-engine components manufactured with nickel-based alloys operate at high temperatures and these conditions cause relaxation of compressive RS generated by peening processes. Therefore, it is necessary to consider the relaxation of RS to reliably design aero-engine components, since expected fatigue performance and corrosion resistance can be effectively reduced. For this reason, some researchers have studied the relaxation of SP induced compressive RS in nickel-based alloys. Khadhraoui et al.[18] studied the relaxation of RS induced by two SP conditions in the nickel-based alloy Inconel 718 at 600 °C and 650 °C for long exposures (10 h and 100 h). They found a significant relaxation of RS in the first period, being maximum at the surface, but the RS pattern was not modified. Later, Prevey et al.[19] compared the relaxation of compressive RS induced by high intensity SP, LSP and gravity peening in Inconel 718 at temperatures ranging from 525 °C to 675 °C for exposure periods from 10 min to 2 000 min. They also observed a higher relaxation of surface RS than subsurface RS without modification of the profile, being this relaxation the highest in SP because it induced the highest degree of cold-work. They found that thermal relaxation of RS occurs in two stages: (A) Rapid relaxation during early stage of the exposure followed by (B) A slower relaxation associated with Avrami diffusion model. MHP also leads to high compressive RS and severe work-hardening, similar to SP, and thus RS relaxation could be relevant. Foss et al.[20] analyzed the relaxation of RS induced by SP in the nickel-based alloy RR1000 at 700 °C for 48 h and they confirmed the conclusions of previous authors. More recently, Li et al.[21] also found a slight relaxation of compressive RS (around 100 MPa) in GH4160 nickel-based alloy specimens treated by four LSP conditions after vacuum annealing at 650 °C for 12 h.

In all cases, thermal relaxation of compressive RS generated by peening were studied *ex-situ* after cooling down. Interestingly, recent investigations have satisfactorily characterized *in-situ* the residual strain relaxation caused by thermal treatments for several materials and applications, showing good agreement with *ex-situ* tests. Most of these studies are focused on the thermal relaxation of RS induced by welding, since this knowledge would enable the optimization of Post-Weld Heat Treatment (PWHT). Chen et al.[22] characterized *in-situ* the residual strain relaxation in the center of butt-welded pipes of C–Mn. They found that residual strains rapidly decrease during initial heat-up and further relaxation occurs when holding at 650 °C, possibly promoted by creep mechanisms. Similarly, Dodge et al.[23] measured significant changes in residual strains in a dissimilar low alloy steel-Alloy 625 weld when heating up to 675 °C, mainly in Alloy 625. Alipooramirabad et al.[24] also reported the highest residual stress relaxation (80%) in the centre of a welded steel plate (API 5L grade X70) during the heating phase, while holding at 650 °C for 60 min, only caused a slight relaxation (11%). Later, they performed *in-situ* neutron diffraction tests to analyze the impact of holding time on the relaxation of RS during PWHT (soaking temperature of 650 °C) for multi-pass high strength low-alloy steel welds and confirmed that holding time is not relevant since most of the RS relaxation occurs during heating phase.[25] Some researchers have carried out *in-situ* experiments in neutron sources to study the thermal relaxation of RS induced by quenching in nickel-based alloys. In a pioneering study, Rolph et al.[26] found a rapid relaxation of about 200 MPa in the hoop and radial directions of water quenched forged nickel-alloy RR1000 samples when ageing at 760 °C, while holding period only caused a slow reduction. Aba-Perea et al.[27] determined that relaxation of RS of water quenched Inconel 718 at 750 °C for 8 h mainly occurs during the heating stage as a result of a combination of plasticity and early stage creep relaxation. Recently, Chen et al.[28] observed that RS induced after oil and water quenching in Inconel 718 were largely relived after 14–20 h exposure at 718 °C, and they observed multistage kinetics of relaxation in their *in-situ* tests.

The literature review has confirmed that MHP can improve the SI of nickel-based alloys. However, the reported findings can be hardly extrapolated to aero-engine critical components because: (A) Some studies did the tests in annealed state of the raw material, and therefore softer material, and (B) MHP was not applied to the machining conditions used in the last stage of the manufacturing chain (turning, hole making or broaching). Furthermore, the range of tested conditions is narrow, and no study has addressed the effect of small diameter tools which can provide: (A) Higher contact pressures leading to higher and deeper compressive RS (even for the age hardened Inconel 718) and (B) Allow treatment of smaller features due to less geometrical constraints (i.e., close to flanges). Additionally, thermal relaxation of RS induced by MHP must be studied to consider in the design of critical aero-engine components. *In-situ* characterization is the most advanced approach, but to the best of the authors knowledge, there is few published *in-situ* experiment analyzing relaxation of machining- and peening-induced RS during early stage of exposure where most of the relaxation occurs.

This paper is aimed at studying the use of small diameter MHP tools to improve the SI of machined nickel-based alloy Inconel 718, widely employed in aero-engine components.[29] In addition, the effect of in-service temperature on SI and thermal relaxation of RS is also analyzed. For this purpose, solution treated, and age hardened Inconel 718 discs were face turned as reference condition, and then a pneumatic hammer peening tool was used to produce eight different surface conditions. Then, the surface topography, RS, nanohardness and microstructure were characterized. To analyze the relaxation of RS, *in-situ* annealing tests were done in the X-ray diffractometer at 550 °C for different exposure periods from 0 to 20 h. Finally, the microstructure characterization and nanoindentation tests were done in the heat-treated samples.

2. Methodology

2.1. Material

The material selected was a nickel-based alloy Inconel 718 bar with a diameter of 118 mm. This was subjected to a structural hardening treatment. The microstructure, chemical composition and mechanical properties of the raw material were

Table 1 Chemical composition of Inconel 718.[30]

Element	Ni	Cr	Fe	Mo	Nb	Ti	Al
Content (wt%)	53.17	18.41	18.45	2.91	5.51	0.99	0.56

characterized in a previous work.[30] The microstructure consisted of austenitic matrix γ with an average grain size of 23 μm, and strengthening precipitates γ′ ($Ni_3(Al,Ti)$) and γ″ (Ni_3Nb). The alloy also had δ-phase precipitates (Ni_3Nb) and carbide particles. The chemical composition and mechanical properties are shown in Table 1[30] and Table 2,[30] respectively.

2.2. Machine hammer peening tests

Four disc-shape specimens with a diameter of 118 mm and thickness of 3 mm were cut by W-EDM from the Inconel 718 bar. Then, both faces of these discs were machined to ensure flatness. One of the faces of the discs was face milled. The other face was turned in a Computer Numerical Control (CNC) lathe prior to MHP tests since this machining process is the reference condition in critical aero-engine components such as turbine discs. Cemented carbide inserts (Mitsubishi DNMG150612) were employed at 70 m/min cutting speed, 0.2 mm feed rate and 0.2 mm depth of cut to face turn the target surface of the discs with coolant supply.

Then, MHP tests were carried out in a Lagun GVC 1000-HS CNC milling machine. Each disc was placed on a triaxial sensor Kistler dynamometer (9139AA) to acquire forces induced during MHP tests. A FORGEfix pneumatic MHP tool was used to treat the surfaces. This tool was clamped in the tool holder of the CNC machine. A total of six surfaces of dimensions 28 mm × 30 mm were hammer peened in each disc. The experimental set-up and the geometry of the specimen are shown in Fig. 1.

Table 2 Mechanical properties of Inconel 718 obtained in compression test.[30]

Parameter	Value
Ultimate compression strength σ_u (MPa)	1 754
Yield strength σ_y (MPa)	1 150
Elastic modulus E (GPa)	206

MHP tests were conducted as follows: (A) The tool with indenter diameter d was moved down an initial off-set of 1 mm, (B) Then the tool moved across the surface in the primary direction at feed rate f, (C) When reaching the end of the path the tool was laterally displaced a stepover distance s, (D) Subsequently the tool moved back at feed rate f along the primary direction and (E) The tool was again displaced a stepover distance s once having reached the edge. Steps B–E were repeated until the entire surface was covered. The schematic of the tool path can be seen in the detail of Fig. 1. The tested MHP conditions are summarized in Table 3. The initial offset (1 mm), hammering frequency (about 250 Hz) and air supply of pneumatic MHP tool (about 600 kPa) were kept constant during the tests. Two different diameters of cemented carbide indenters (4 mm and 12 mm), two different feed rates (2.5 m/min and 5.0 m/min) and stepover distances (0.07 mm and 0.35 mm) were used in the MHP tests. Thus, a total of 8 conditions were tested, and 3 repetitions of each.

2.3. Surface integrity characterization

The SI characterization was divided in two stages. First, surface topography and surface RS of all treated surfaces were measured. Those MHP conditions that generated an arithmetic average roughness $Ra < 0.8$ μm (aeronautic industry

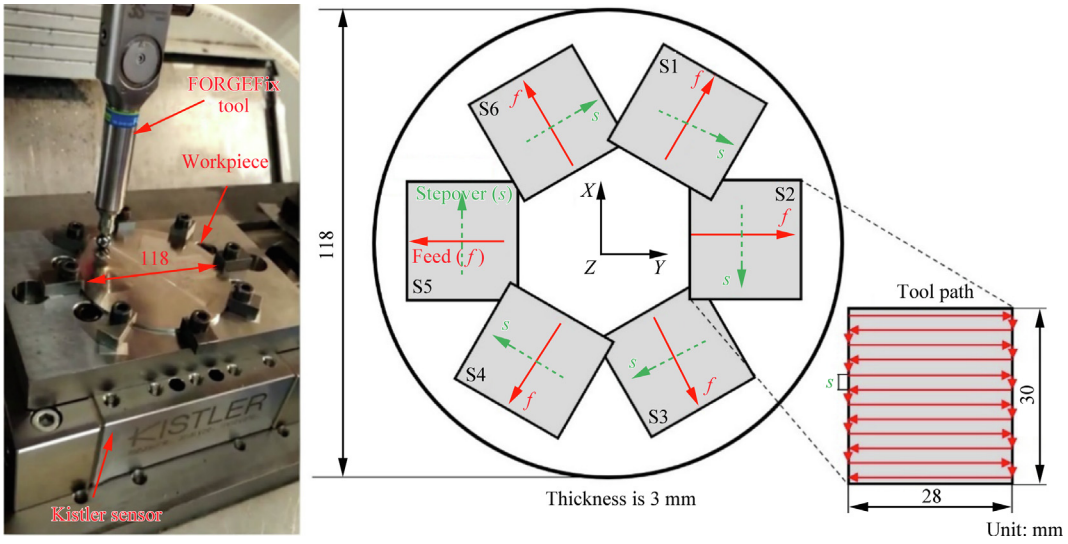

Fig. 1 Experimental set-up, geometry of disc-shape specimen with distribution of hammer peened surfaces and identification of feed rate (f) and stepover direction (s), and a schematic of tool path during hammer peening.

Table 3 Parameters of MHP tests.

d (mm)	f (m/min)	s (mm)
12	2.5	0.07
		0.35
	5.0	0.07
		0.35
4	2.5	0.07
		0.35
	5.0	0.07
		0.35

specification for safety critical components)[15] and induced compressive RS, were selected for the next step, since the study is aimed at enhancing the SI of Inconel 718 alloy components. In the second step, a more detailed SI characterization was conducted. Subsurface RS were measured in the selected MHP conditions and turned surface as reference. The microstructure of the affected surface layer was analyzed by Scanning Electron Microscopy (SEM) and the variation of mechanical properties from the treated surfaces to the bulk was assessed by the nanoindentation technique. The following paragraphs describe in detail the methods.

The surface topography was characterized using two different techniques. On the one hand, the portable roughness tester Mitutoyo SJ-210 was employed to obtain *Ra*, *Rq*, *Rz*, and *Rt* 2D roughness indicators following the ISO standards 4287 and 4288. The tip radius of the contact surface roughness tester was 5 μm. At least three measurements were taken in the feed and stepover directions. On the other hand, the optical profilometer Alicona IFG4 was used to obtain the 3D surface topography. An area of about 4 mm × 4 mm was measured from each surface using 20× magnifications. Hence, 80 images were taken from each surface to generate the 3D area. The vertical and lateral resolutions were set to 200 nm and 2 μm, respectively. As a result, around 95 million points make up each measured surface. The resolutions and the size of the measurement area were selected based on the recommendations on the equipment manual.

Surface RS of the 24 hammer peened surfaces (8 conditions, 3 repetitions) were measured in the feed and stepover direction by the X-Ray Diffraction (XRD) technique using a portable Proto iXRD equipment. These measurements were done at three points located at the center of each surface, which were separated by 2 mm. MnKα radiation was used (wavelength $\lambda = 2.103$ Å), with a voltage of 20 kV and current of 4 mA. A round collimator of 1 mm diameter was used to narrow the irradiated area. The beam was tilted at eleven positions from $\psi = -41°$ to $\psi = 41°$ to apply the $\sin^2\psi$ method. At each tilting angle 10 exposures of 1 s were carried out to collect data of (311) diffraction peak. Experimental data was analyzed by means of PROTO XrdWin software. The diffraction elastic constants S_1 and S_2 used in the measurements were

$$-S_1 = -\nu/E = 1.61 \times 10^{-6}\,\mathrm{MPa}^{-1} \quad (1)$$

$$1/2\,S_2 = (1+\nu)/E = 7.14 \times 10^{-6}\,\mathrm{MPa}^{-1} \quad (2)$$

where ν is Poisson's ratio.

Subsurface RS were measured at the center of the selected surfaces and turned surface. For this purpose, surface layers were removed by electropolishing. After each layer removal step, the depth was verified using a contact profilometer and RS were measured in the feed and stepover direction employing the procedure described in the preceding paragraph. A total of 12-layer removal steps were conducted to measure the variation of RS from the surface to approximately 800 μm depth.

To analyze the microstructure of the surface layer affected by the selected conditions and turning as reference, samples were extracted from the discs by W-EDM. Then, smaller samples were cut using a metallographic saw. Those samples were hot mounted in a phenolic resin with carbon filler, ground and polished. The last step was polishing with an active colloidal silica suspension (0.05 μm particles). Then, samples were electro-etched with 10vol% oxalic acid solution. A FEI Quanta 650 FEG-SEM Scanning Electron Microscope was employed to analyze the microstructure of the turning- and hammer peening-affected layer. Images were obtained at different magnifications using a 20 kV voltage and working distance of approximately 10 mm. Complementarily, a second batch of samples was prepared using the same procedure up to the final polishing step. Those samples were characterized using the Electron Backscatter Diffraction (EBSD) technique in the same microscope. In each sample, a surface area of 150 μm × 250 μm was characterized using a step size of 0.5 μm. Finally, EBSD data was analyzed using Aztec Crystal software.

The variation of mechanical properties (reduced elastic modulus E_r and hardness H) within the hammer peening affected layer were determined by the nanoindentation technique using a Bruker/Hysitron TS77 Select equipment. The samples prepared for the EBSD analysis were used in the nanoindentation tests since they require a flat surface. All nanoindentations were done using a Berkovich tip under displacement control, performing indentations up to a 200 nm depth and then releasing. These conditions required a spacing of 5 μm between indentations to avoid side effects. This spacing is not enough to study the main changes occurring near the surface. For this reason, the measurements were done using two different scan lines. The first scan line was tilted about 11° with respect to the surface, and this allowed us to do nanoindentations with increments of 1 μm in the perpendicular direction to the treated surface up to a 20 μm depth. The second scan line was conducted perpendicular to the treated surface from 20 μm to 500 μm depth with a spatial resolution of 5 μm. Data was processed using the Hysitron Triboscan software and the Oliver Pharr method.[31]

2.4. In-situ annealing tests

In-situ annealing tests were done in the Proto iXRD machine to determine the evolution of RS for different exposure periods at 550 °C (reference in-service temperature provided by an aero-engine manufacturer). The experimental set-up is shown in Fig. 2. Specimens with dimensions 20 mm × 20 mm × 3 mm of the selected MHP conditions were cut out from the discs by W-EDM. These were placed on the Anton Paar DHS 900 heating stage and covered with a plastic dome to

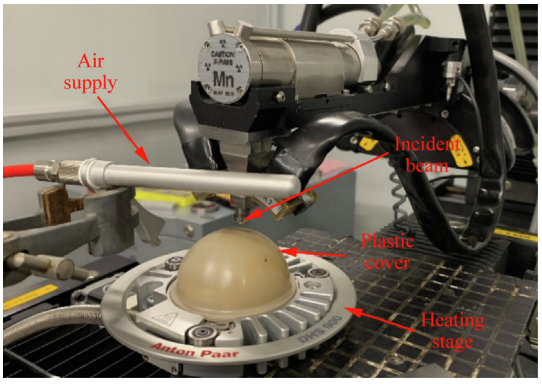

Fig. 2 Set-up of *in-situ* annealing tests in Proto iXRD equipment.

avoid heat dissipation. Specimens were heated up at 10 °C/min rate in air at ambient pressure. The plastic cover was cooled down by air supply. Heating was interrupted at 200, 300, 400, 450, 500 °C for 10 min to measure RS changes during early exposure. Once reaching the target temperature of 550 °C, RS were measured for different exposure periods: 0, 0.5, 1.0, 1.5, 2.0, 2.5, 3.0, 3.5, 4.0, 4.5, 20.0 h. Then, the plastic dome was removed, and the specimen cooled down in air up to Room Temperature (RT), and a final RS measurement was done.

During the *in-situ* annealing test RS were measured using the $\sin^2\psi$ method following the procedure described in Section 2.3. However, at each tilting angle, 40 exposures of 1 s were taken since the plastic dome attenuates the incident and upcoming X-ray beam. Consequently, this increased the measurement time and RS were only measured in the stepover direction (highest magnitude of RS). In fact, RS measurements in two directions would have taken excessive time and they would have overlapped the short thermal exposure periods (0 and 0.5 h). The second important consideration in the *in-situ* annealing tests was the change of diffraction elastic constants with temperature. The elastic constants for (311) diffraction were calculated from the work carried by Aba-Perea et al.,[32] where elastic diffraction constants of Inconel 718 were determined by combining thermal tests and neutron diffraction measurements. These values are shown in Table 4.[32]

Finally, small samples were extracted from the specimens used in the *in-situ* annealing tests and prepared to observe in the SEM and perform nanoindentations tests employing the procedure described in Section 2.3.

3. Results

3.1. Machine hammer peening forces

The forces induced during MHP tests were measured using the set-up of Fig. 1. The Kistler dynamometer measured forces in the absolute axis X, Y and Z shown in Fig. 1. Since the treated surfaces had a different orientation with respect to the absolute coordinate system, forces were then calculated in the local reference system of each MHP section for the feed, stepover and perpendicular to the surface (Z) direction for comparison.

Fig. 3 shows the average of the peak forces measured in the three directions, and they include the standard deviation bar. The highest peak forces were induced in the perpendicular direction to the surface because of the impacts, and they ranged from 625 N to 725 N. There is not a clear effect of the tested feed and stepover parameters on the perpendicular peak forces ($F_{Z,\ max}$), and an increase in tool diameter slightly reduces $F_{Z,\ max}$. Furthermore, the magnitude of forces is similar to the values obtained when hammer peening aluminum with the same set-up.[33,34] This suggests that the forces in the perpendicular direction to the surface mainly depend on the pressure applied to the pneumatic hammer peening tool. Besides, forces induced by MHP were considerably higher

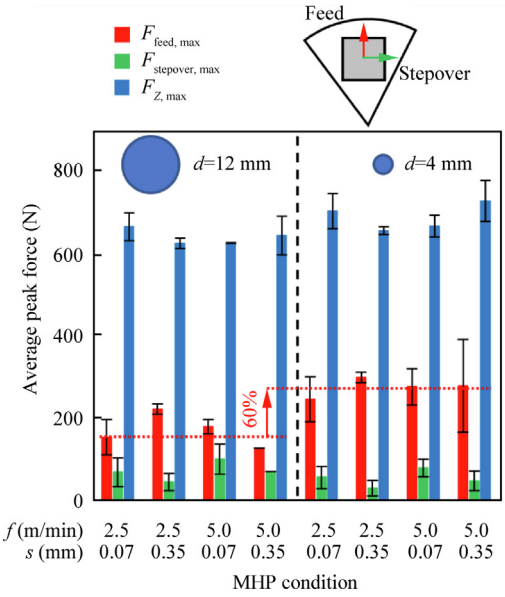

Fig. 3 Average peak forces induced by tested MHP conditions.

Table 4 Diffraction elastic constants of peak (311).[32]

Temperature (°C)	E_{311} (GPa)	ν_{311}	$-S_1$ (10^{-6} MPa^{-1})	$1/2\ S_2$ (10^{-6} MPa^{-1})
RT	203	0.29	1.61	7.14
200	190	0.34	1.79	7.05
300	185	0.34	1.84	7.24
400	182	0.35	1.92	7.42
450	180	0.35	1.94	7.50
500	177	0.34	1.92	7.57
550	168	0.34	2.05	7.98

(150–250 N) in the feed direction ($F_{\text{feed, max}}$) than in the stepover direction ($F_{\text{stepover, max}}$). Feed forces are mainly caused by the friction between the indenter and workpiece in the main sliding direction. It can be clearly seen that forces in the feed direction increased on average 60% when using the tool with the smallest diameter since contact pressure and friction forces increase. However, the effect of feed rate and stepover distance on $F_{\text{feed, max}}$ and $F_{\text{stepover, max}}$ forces was not relevant considering the standard deviation.

3.2. Surface topography

Fig. 4(a) shows the roughness measured with the contact surface roughness tester in the feed and stepover directions. The roughness produced by turning is highly dependent on the direction of measurement due to the kinematic effect of the tool. For instance, *Ra* is approximately 0.15 μm in the cutting direction and 0.82 μm in the feed direction. After applying the MHP treatment, the roughness tends to equalize in both directions. This fundamentally occurs because MHP flattens the peaks generated by turning, producing a more homogeneous surface. Nonetheless, as can be observed from the 3D surface topography in Fig. 4(b), depending on the MHP conditions, and particularly the indenter diameter, the machining feed marks may still be visible (surfaces treated with $d = 12$ mm), or a completely new topography may be created by the indenter geometry (surfaces treated with $d = 4$ mm). Therefore, the roughness varies significantly depending on the MHP conditions.

In all cases, MHP homogenizes the machined surface by flattening the peaks produced by the cutting tool. This always results in an improvement of the roughness in the feed direction, while in the stepover direction its improvement/deterioration depends on the MHP conditions. The indenter diameter and the stepover distance are the two parameters that most influence the surface topography.

All the observations regarding roughness indicators are corroborated by the 3D surface topography results (see Fig. 4(b)). The topography undergoes a complete transformation from the machined surface to the MHP surfaces. Furthermore, variations in the indenter diameter are more pronounced

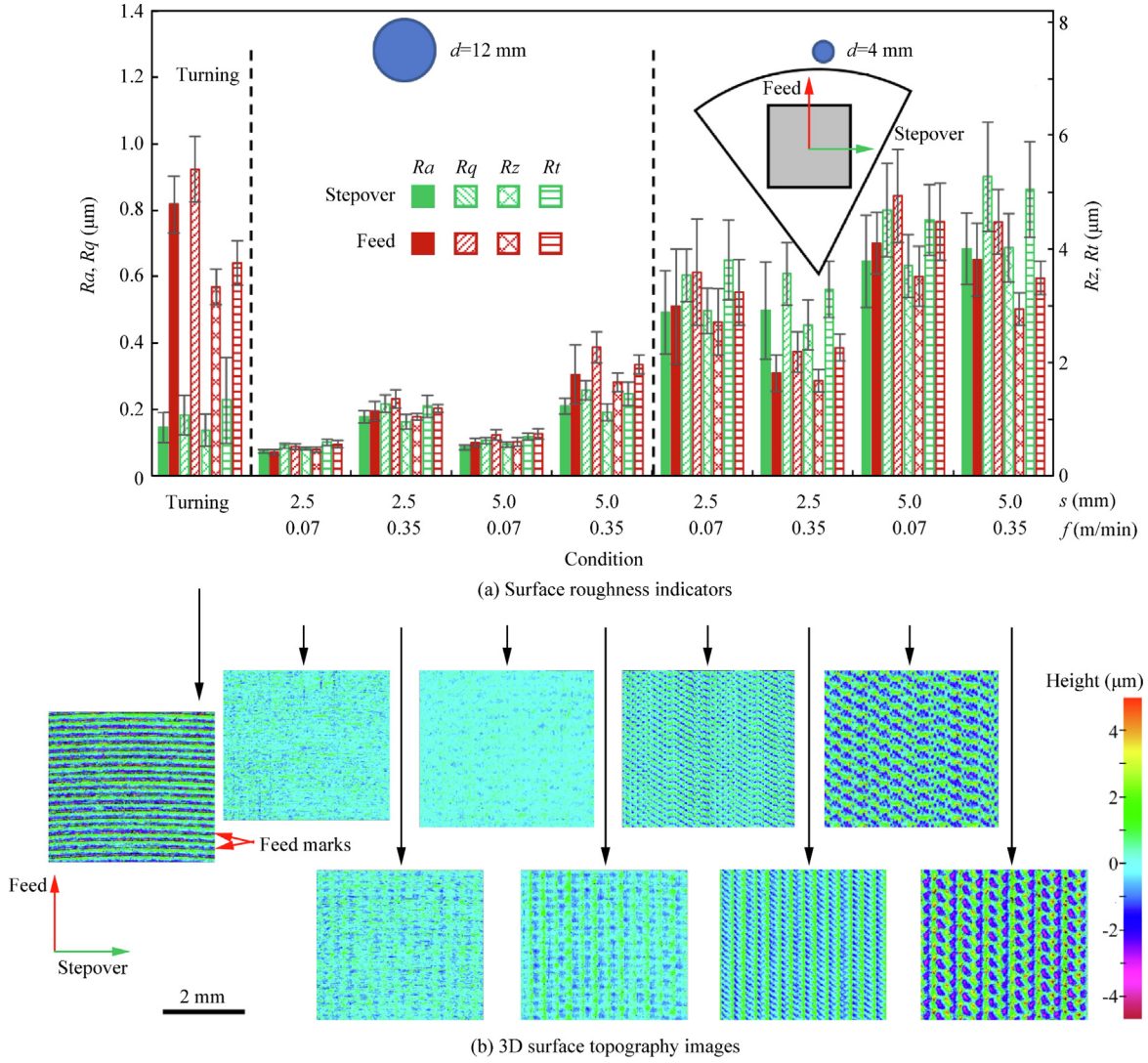

Fig. 4 Surface roughness indicators and 3D surface topography generated by turning and tested MHP conditions.

compared to those resulting from changes in the stepover distance and feed rate.

3.3. Residual stresses

Fig. 5 shows the RS induced by face turning and tested MHP conditions. The magnitude of RS represents the mean value for each surface condition and the bars depict the standard deviation.

Face turning operation generated high tensile RS in the cutting direction (977 ± 262 MPa) and feed direction (581 ± 254 MPa). Surface RS generated by cutting are a consequence of two main effects: (A) Mechanical effect associated with cutting forces, which leads to more compressive RS, and (B) Thermal effect that induces more tensile RS. Thus, the results evidence that the thermal effect was dominant for the tested conditions as reported by other authors.[5] This is expected in nickel-based alloys since they have low thermal conductivity, and a high amount of heat is generated during the cutting process.

Tested MHP conditions reduced the magnitude of tensile RS induced by machining or even converted into compressive RS. Interestingly, compressive RS were generated when using the tool with the smallest diameter, with mean values ranging from –592 MPa to –1 435 MPa in the stepover direction and from –273 MPa to –666 MPa in the feed direction. The highest compressive RS were generated when using the smallest stepover distance (s = 0.07 mm). These conditions produced higher RS than the yield stress of the material (1 150 MPa), which suggests that the surface must have been work hardened. However, only one surface treated with the 12 mm diameter tool (f = 5.0 m/min and s = 0.07 mm) showed compressive RS. Therefore, these results confirm that small diameter tools can generate high compressive RS because high contact pressures are induced in the smallest contact region.

Considering the surface topography criteria (Ra < 0.8 µm) and surface RS criteria (compressive RS) described in Section 2.3, four conditions were selected for the next step: (A) d = 12 mm, f = 5.0 m/min and s = 0.07 mm; (B) d = 4 mm, f = 2.5 m/min and s = 0.07 mm; (C) d = 4 mm, f = 5.0 m/min and s = 0.07 mm; (D) d = 4 mm, f = 5.0 m/min and s = 0.35 mm. It should be noted that one of the conditions tested with the smallest diameter was not selected because it induced lower compressive RS and the results exhibited significantly higher scatter than the rest of the conditions.

Fig. 6 compares the RS profiles generated by the turning process (initial state) and the selected MHP conditions. It should be clarified that the cutting direction (hoop direction) was almost parallel to the stepover direction. Turning process induced the typically reported hook shape profile: tensile RS near the surface (980 MPa in the cutting and 870 MPa in the feed direction) which rapidly decreased in a shallow layer (about 40 µm) up to a maximum compressive RS (–690 MPa in the cutting and –490 MPa in the feed direction), and finally they relaxed and stabilized within the bulk material at about 150–200 µm depth.

Importantly, all the selected MHP conditions induced higher compressive RS and a thicker compressive layer (about 500–700 µm thick) than turning. Therefore, these results confirm that optimized MHP can overcome the RS generated by machining in nickel-based alloys, leading to a more favorable RS state. Furthermore, the 4 mm diameter tool induced higher compressive RS than high intensity SP in Inconel 718[8] within a 2–3 times thicker compressive RS layer.

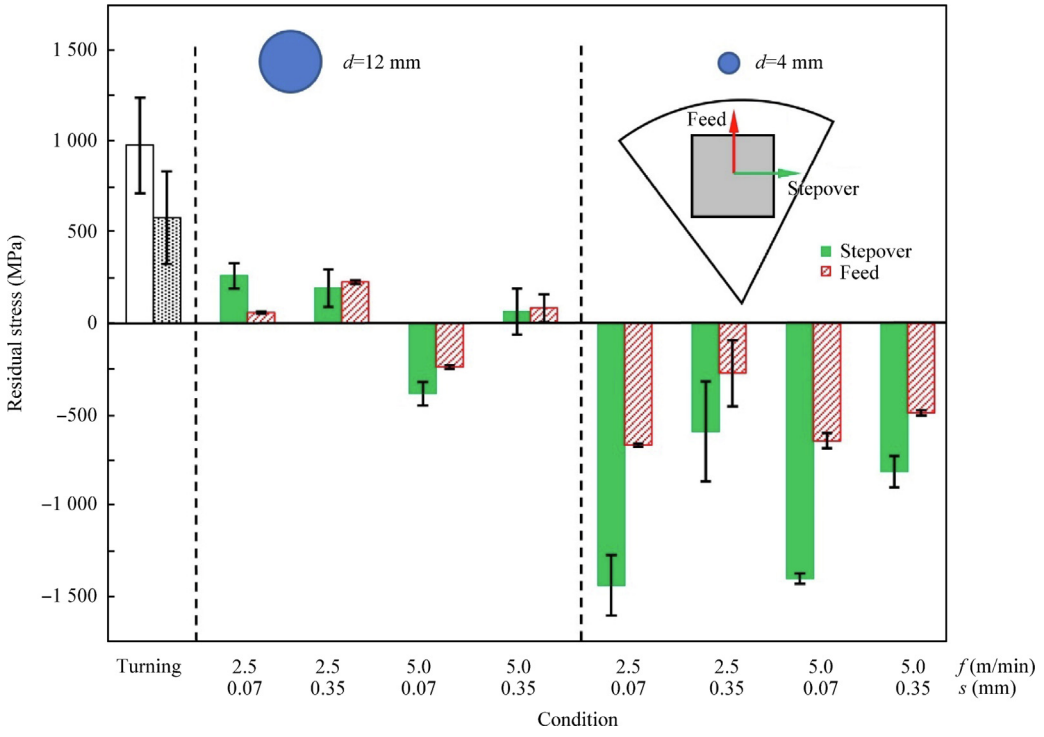

Fig. 5 Surface RS induced by turning and tested MHP conditions.

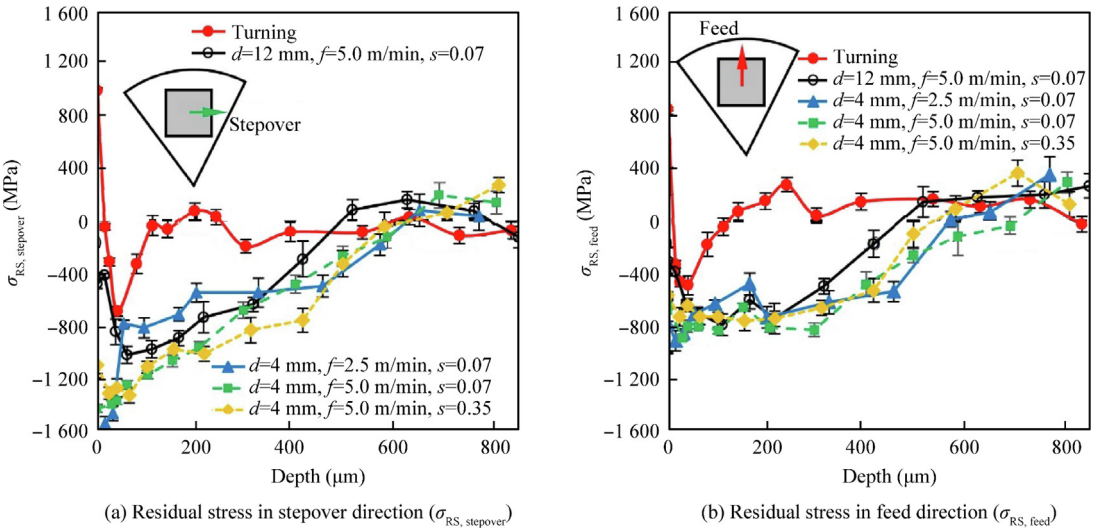

(a) Residual stress in stepover direction ($\sigma_{RS,\ stepover}$) (b) Residual stress in feed direction ($\sigma_{RS,\ feed}$)

Fig. 6 RS profiles generated by turning and selected MHP conditions in stepover direction and feed direction.

The RS profiles induced by the selected conditions when using the 4 mm diameter tool follow a similar pattern and comparable RS within the material, although a different behavior is detected within the first 50 μm. In the stepover direction, RS were the most compressive near the surface and they gradually reduced their value up to about 500–700 μm depth. By contrast, a compressive RS plateau (from –600 MPa to –800 MPa) can be observed in the feed direction up to about 300–400 μm, and then, they rapidly decreased to reach bulk values. The 12 mm diameter tool induced the maximum compressive RS at 50 μm depth, and then followed the same RS pattern. In all cases, low tensile RS were induced at higher depths to balance the compressive RS.

3.4. Microstructure

Fig. 7 shows the images of the microstructure affected by turning and the selected MHP conditions. The microstructure was analyzed in the cutting direction of the turned sample and stepover direction of the MHP samples because these directions showed the highest magnitude of RS.

The initial face turning process generated a continuous thin white layer (2 μm thick), as can be seen in Figs. 7(a) and (b). Below the white layer, there is also a region with severe deformation, evidenced by slip bands. As consequence of the severe deformation, some of the grains were bent near the surface, but this deformation did not exceed 20 μm in depth.

The microstructure affected by the selected MHP conditions is shown in Figs. 7(c)–(f). The white layer and severely deformed layer (indicated by dashed line) generated by the preceding turning process are still visible. Although RS profiles demonstrated that the effect of MHP covered a deeper region, selected MHP tests did not generate additional severe deformation since the maximum deformation of grains did not exceed 20 μm in depth. An isolated cracked carbide can be observed in the microstructure affected by MHP with the 12 mm diameter tool at feed rate of 5.0 m/min and stepover of 0.07 mm (see Fig. 7(c)). However, an irregular surface was generated when using the smallest diameter which led to a higher roughness in the stepover direction as can been seen in Fig. 4.

To further analyze the effect of turning and MHP on the microstructure, the EBSD technique was used. Particularly, the Kernel Average Misorientation (KAM) parameter was studied. Dislocations induced by plastic deformation lead to a misorientation, and for this reason KAM has been widely applied to study layers with Severe Plastic Deformation (SPD). Fig. 8(a) shows two examples of KAM maps of selected MHP conditions. It should be clarified that KAM maps were overlap with the image taken in the SEM. This allowed us to quantify the average thickness of the non-indexed region, which can be attributed to a highly deformed and distorted layer, or recrystallized layer with nanograins. As can be seen in the two examples, there was a non-indexed region ranging from 5 μm to 10 μm. This thickness correlates with the presence of the white layer and severely deformed layer reported in Fig. 7. Below this region, high values of KAM are present, which gradually decrease when increasing the depth. Grain Boundaries (GB) also accommodated more dislocation as KAM value increased in this region.

The KAM distribution across the most deformed region of the turned specimen and selected MHP condition is compared in Fig. 8(b). In all cases, the non-indexed region associated with the presence of white layer and severely deformed layer was similar. The variation of KAM across the depth of the specimens followed the same trend. This decreased exponentially until reached a stable low KAM value at about 60 μm depth. Almost all tested surfaces showed a similar behavior, but the surface treated with the 4 mm diameter tool at feed rate 2.5 m/min and stepover 0.07 mm, showed higher KAM values within the affected thickness. This is also evident on the right map of Fig. 8(a). The preceding SEM analysis in Fig. 7 revealed deformed grains within the first 20 μm. The KAM analysis suggests that the severe plastic deformation (considering this is the main source for the motion of dislocations caused during MHP) is deeper (about 60 μm), but the steepest decrease of KAM value agrees with the deformation of the grain (about 20 μm).

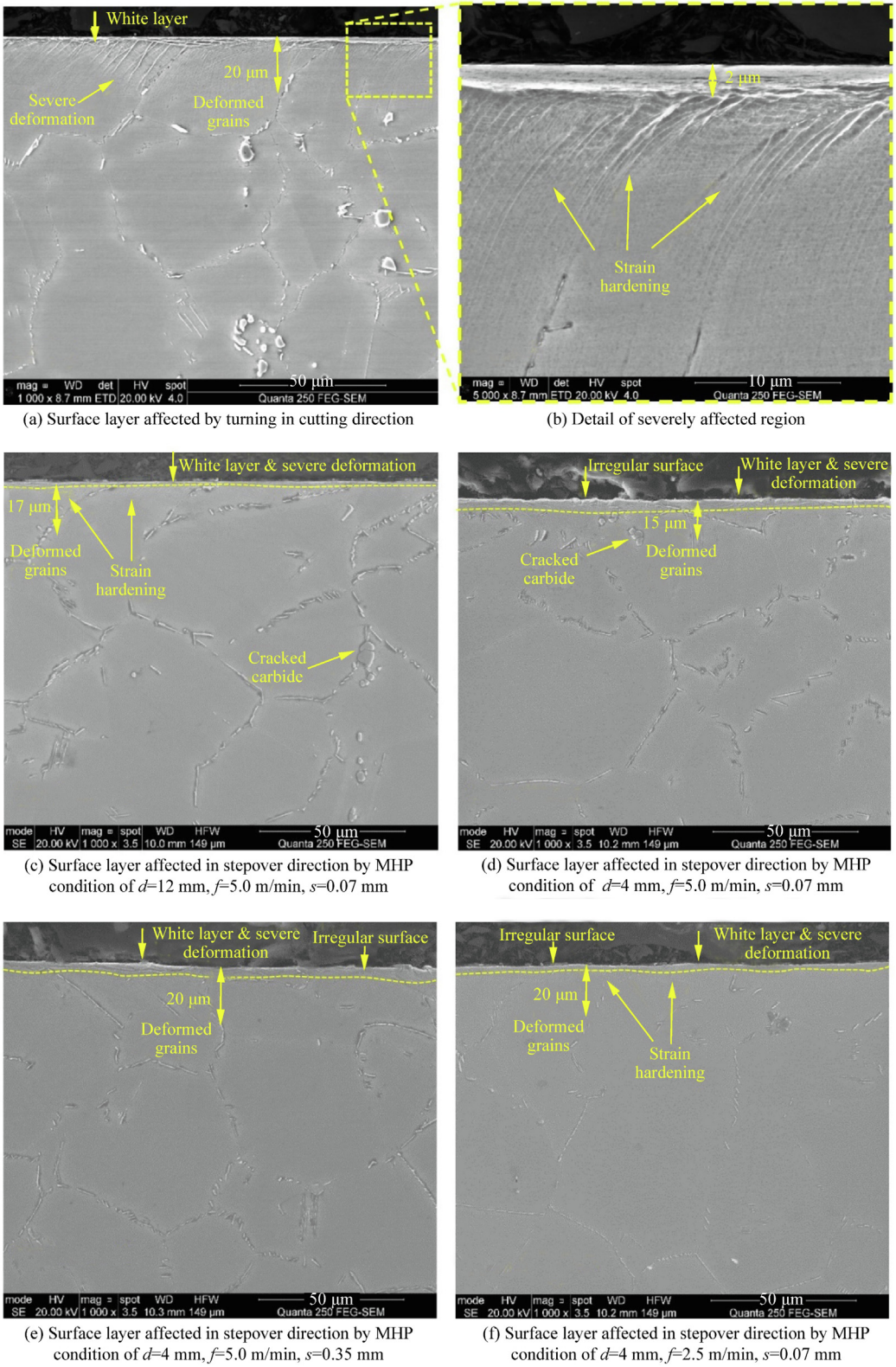

(a) Surface layer affected by turning in cutting direction

(b) Detail of severely affected region

(c) Surface layer affected in stepover direction by MHP condition of d=12 mm, f=5.0 m/min, s=0.07 mm

(d) Surface layer affected in stepover direction by MHP condition of d=4 mm, f=5.0 m/min, s=0.07 mm

(e) Surface layer affected in stepover direction by MHP condition of d=4 mm, f=5.0 m/min, s=0.35 mm

(f) Surface layer affected in stepover direction by MHP condition of d=4 mm, f=2.5 m/min, s=0.07 mm

Fig. 7 Secondary electron images of microstructure of surface layer affected by turning in cutting direction, and by different MHP conditions in stepover direction.

X-ray diffraction measurements can also be used to determine the degree of plastic deformation. It is widely accepted that the width of the diffracted peak, typically characterized by the Full Width at Half Maximum (FWHM), is a good indicator of the level of plastic deformation.[35,36] Although the FWHM is not solely linked to the plastic deformation, it

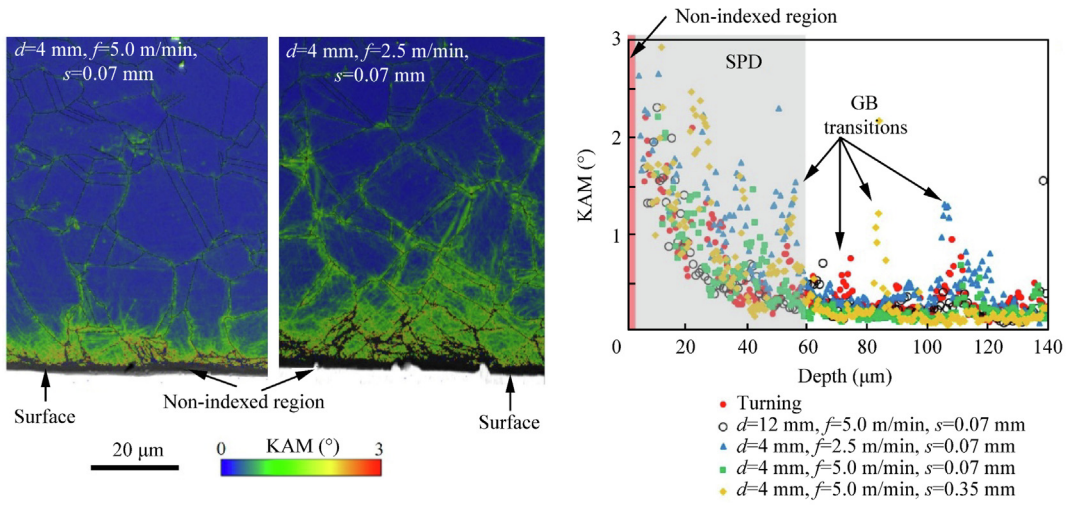

(a) Examples of KAM maps of selected MHP conditions at initial state

(b) Distribution of KAM across depth within region with maximum deformation

Fig. 8 Examples of KAM maps of selected MHP conditions at initial state and distribution of KAM across depth within region with maximum deformation of turned and MHP samples.

increases when the degree of plastic deformation increases. Nickel-based alloys are prone to work-hardening and FWHM can considerably increase with respect to the bulk value in machined and peened surfaces.[8,35,37]

Fig. 9 compares the normalized FWHM profiles (local FWHM with respect to the bulk FWHM ($FWHM_{bulk}$)) of the turned and MHP samples. Normalized FWHM profiles followed the same trend: highest values and changes occurred within 20 μm, in agreement with the severe plastic deformation observed in the SEM and KAM analysis. FWHM reached the bulk value at about 100 μm depth in the turned surface, while it was stabilized at about 400 μm depth in the MHP surfaces.

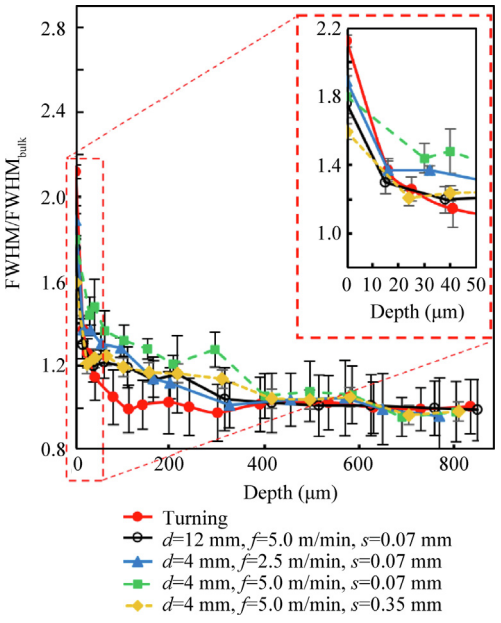

Fig. 9 FWHM profiles generated by turning and selected MHP conditions.

These results suggest that FWHM is more sensitive than KAM to detect lower degrees of plastic deformation, as also found by Foss et al.[20] when analyzing the effect of SP on nickel-based alloy RR1000.

3.5. Nanohardness

The reduced modulus (E_r) and hardness (H) of the selected hammer peened surfaces characterized by nanoindentation tests are shown in Fig. 10. The main changes occurred near the surface and then, E_r and H were stabilized within the bulk material. For this reason, Fig. 10 are plotted up to 100 μm depth despite measuring across 500 μm depth. Lines have been added to guide the reader.

All tested conditions showed a 10%–20% decrease of the reduced modulus E_r within about 15 μm depth at the initial state (Fig. 10(a)). It is more difficult to define trends from the hardness H profile due to the scatter of results near the surface (Fig. 10(b)). There is a slight increase of hardness (10%–15% on average) within 20 μm depth when employing a feed rate of 5.0 m/min and stepover of 0.07 mm with both tools. However, the two others selected MHP conditions did not evidence such an increase of hardness near the surface.

3.6. In-situ annealing tests

The heating up process was stopped at certain temperatures and hold for 10 min to measure surface RS. Fig. 11(a) shows the changes in surface RS in the stepover direction from room temperature to 550 °C characterized by combining *in-situ* annealing tests and X-ray diffraction measurements. It should be noted that surface RS were analyzed in the feed direction of the specimen treated with the 4 mm diameter tool at feed rate 2.5 m/min and stepover 0.07 mm due to an incorrect orientation of the specimen in the *in-situ* annealing test. Nevertheless, this does not obscure the findings of this experiment. Surface RS of the four selected conditions followed the same trend as can be seen in Fig. 11(a). At the beginning of the heating

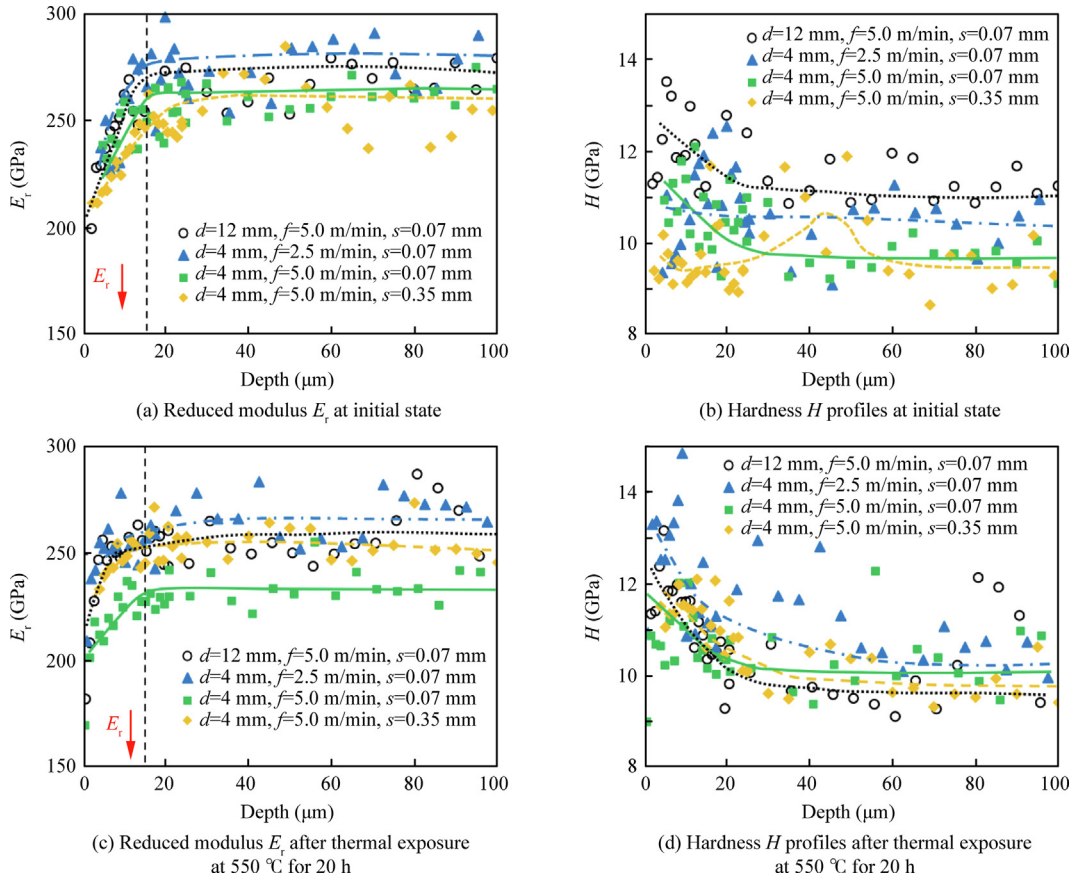

(a) Reduced modulus E_r at initial state

(b) Hardness H profiles at initial state

(c) Reduced modulus E_r after thermal exposure at 550 ℃ for 20 h

(d) Hardness H profiles after thermal exposure at 550 ℃ for 20 h

Fig. 10 Reduced modulus E_r and hardness H profiles of selected MHP surfaces at initial state and after thermal exposure at 550 °C for 20 h.

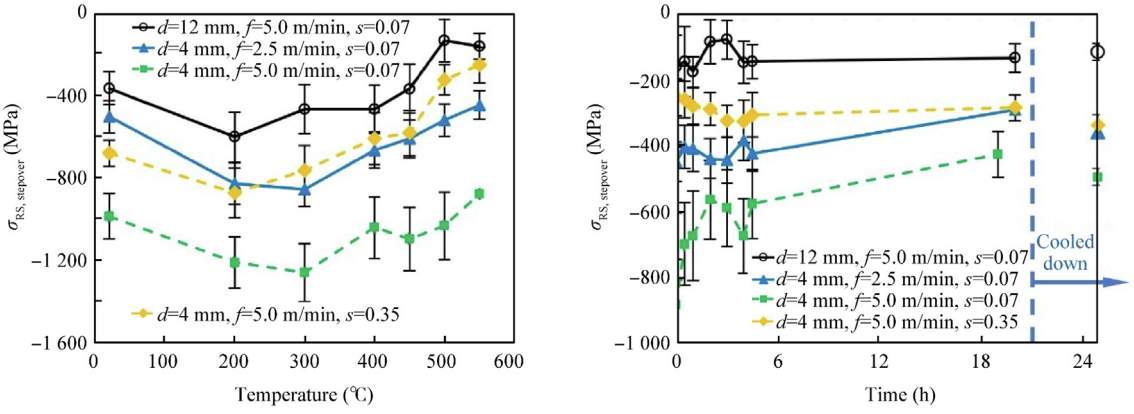

(a) Surface RS in stepover direction of selected MHP conditions during heating up process

(b) Evolution of surface RS in stepover direction during thermal exposure at 550 ℃ and after cooling down

Fig. 11 Surface RS in stepover direction of selected MHP conditions during heating up process and evolution of surface RS in stepover direction during thermal exposure at 550 °C and after cooling down.

up process (up to 200–300 °C) RS became more compressive, possibly caused by the initial transient behavior. Surface RS started slightly relaxing at 300 °C, and the relaxation rate was higher above 450 °C. The relaxation ranged from 15% to 60% during the heating up process. However, all tested conditions exhibited a comparable relaxation (50%–70%) at temperatures above 300 °C.

Fig. 11(b) shows the evolution of surface RS of the MHP surfaces at 550 °C and after cooling down in air. In most cases, the variation of surface RS was negligible within the first 4 h of

exposure since those variations are within the uncertainty of measurements. However, surface RS were relaxed about 25% in the sample with most compressive RS. A longer exposure also caused further relaxation in the sample with the highest RS, while they remained stable when initial compressive RS was smaller than –400 MPa. Finally, it can be seen that RS remain compressive after cooling down and they are similar to those at 550 °C after 20 h of exposure. This correspondence was also found by Aba-Perea et al.[27] by *in-situ* RS analysis in quenched Inconel 718 during annealing treatments at 750 °C using neutron diffraction.

The microstructure of the selected MHP conditions in the stepover direction after thermal exposure can be observed in Fig. 12. The long thermal exposure did not affect the microstructure of the bulk property. The white layer and severely deformed layer found at the initial state was still present, with a thickness ranging from 1 μm to 6 μm. After thermal exposure, a higher number of precipitates was visible within the severely deformed layer as can be seen in the details of Figs. 12(b) and (f). Chen et al.[14] also found a higher amount of γ'/γ'' precipitates in the surface layer of hammer peened oil grade Inconel 718 after annealing.

Fig. 13(a) shows two examples of KAM maps of selected MHP conditions, and Fig. 13(b) compares the distribution of KAM across the most deformed region of all the selected MHP conditions after the thermal exposure. The KAM maps evidenced a slight reduction of the thickness of the non-indexed region and a reduction of the region with higher KAM values. The variation of KAM across the depth of the specimens followed the same trend of the initial state. However, the magnitude of KAM values decreased about 0.5° near the surface, as well as the gradient of the changes and the affected thickness from about 60 μm to about 45 μm. The KAM values in the transition of grain boundaries also showed lower values. These reductions were consequence of the relocation of dislocations induced by the long thermal exposure.

The reduced modulus (E_r) and hardness (H) of the selected MHP surfaces after thermal exposure at 550 °C are shown in Figs. 10(c) and (d) respectively. They followed a similar trend to the initial state. All tested conditions showed a decrease of the reduced modulus E_r within about 15 μm compared to the bulk, as observed at the initial state (Fig. 10(a)). The E_r of the bulk material was slightly affected by the thermal exposure since it decreased around 5%–10% (10–30 GPa) compared to the initial state. Hardness H profiles showed less scatter after thermal exposure than at the initial state. In all tested sample, there was a slight increase of hardness (10%–13% on average) within 20 μm depth. Some authors have shown that white layers and severely deformed layers in nickel-alloys are formed by nanosized grains,[38] which explains the increase in hardness.

4. Discussion

4.1. Effect of MHP conditions on surface integrity

Pneumatic MHP modified the initial surface topography and RS field induced by the turning process. However, the microstructure near the surface was not significantly altered as evidenced by SEM images, KAM analysis and nanohardness measurements. For this reason, we discuss the effect of MHP conditions on surface topography and RS state.

Surface topography is mainly affected by the indenter diameter and the stepover distance. Using an indenter diameter of 4 mm improves the roughness in the feed direction but worsens in the stepover direction in comparison with turning. In contrast, the indenter of 12 mm significantly improves the surface roughness in both directions. Both tools apply similar force, but the contact pressures are higher when using the smallest diameter which induces higher surface deformation.

Regarding the impact of stepover distance and feed rate, their influence is less pronounced compared to the indenter diameter. In general, increasing the feed rate and stepover distance tends to worsen the surface roughness due to a decrease in the hammering frequency per unit of surface. As the hammering frequency is constant (about 250 Hz) when increasing the feed rate, it reduces the impacts per unit length in the feed direction. Similarly, the increase in stepover distance leads to fewer passes being made in the treated surface in the stepover direction, thereby reducing the number of impacts in that direction and consequently worsening the surface roughness.

In any case, MHP homogenizes the surface, which can improve fatigue life by reducing the stress concentration factor, and also equalizes the properties of the surface in both directions, improving the isotropic behavior of the component. Furthermore, even with the smaller diameter indenter, the roughness in both directions remains below the threshold set by the aerospace industry for critical components ($Ra < 0.8$ μm).

Tested MHP conditions induced compressive RS up to 500–600 μm depth, while the machining-affected layer was about 150 μm thick (Fig. 6). Sliding concentrated contacts, such as those developed in continuous contact pneumatic MHP tests, are subjected to Hertzian theory.[39] The contact force F_Z was higher than the force in the feed direction (F_{feed}) and stepover direction ($F_{stepover}$). Thus, the Hertzian contact is a good indicator for the generation of residual stresses. If a contact force P is applied to two elastic spheres of radii R_1 and R_2, the circular contact region has a radius a. This radius can be determined from classical Hertz analysis using[40]

$$a = \left(\frac{3\pi P R}{4E^*}\right)^{\frac{1}{3}} \tag{3}$$

where E^* is composite contact modulus.

The composite radius R is obtained using

$$\frac{1}{R} = \frac{1}{R_1} + \frac{1}{R_2} \tag{4}$$

Similarly, the composite contact modulus E^* can be obtained using

$$\frac{1}{E^*} = \frac{1-\nu_1^2}{E_1} + \frac{1-\nu_2^2}{E_2} \tag{5}$$

where E_1, ν_1, E_2 and ν_2 are the elastic modulus and Poisson's ratio of Spheres 1 and 2, respectively.

Then, the contact pressure p_0 can be calculated employing

$$p_0 = \frac{3P}{2\pi a^2} \tag{6}$$

Applying von Mises criteria, yielding will occur in the sphere with the lowest yield stress Y, when the pressure exceeds $(p_0)_y$. This can be calculate using

$$(p_0)_y = 1.40\,Y \tag{7}$$

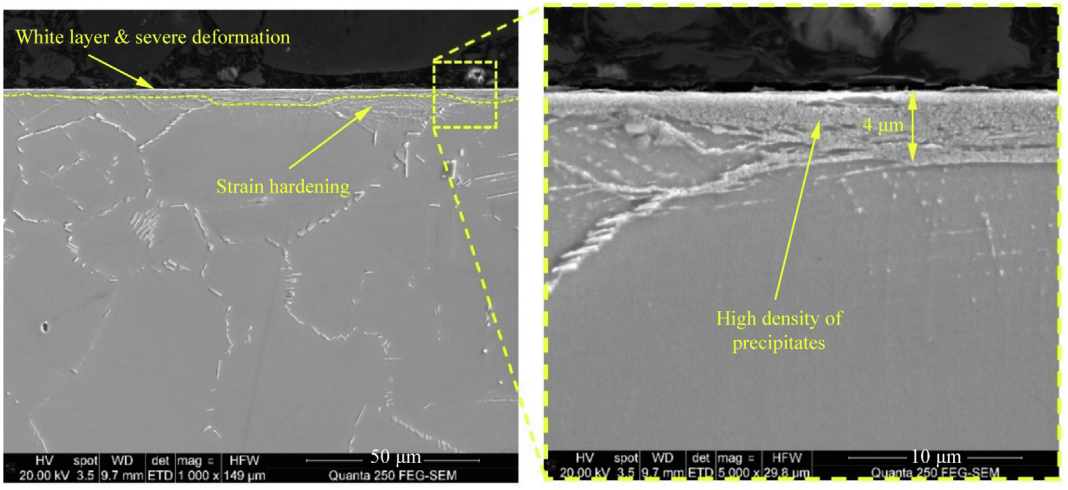

(a) d=12 mm, f=5.0 m/min, s=0.07 mm (b) Enlarged view of Fig. 12(a)

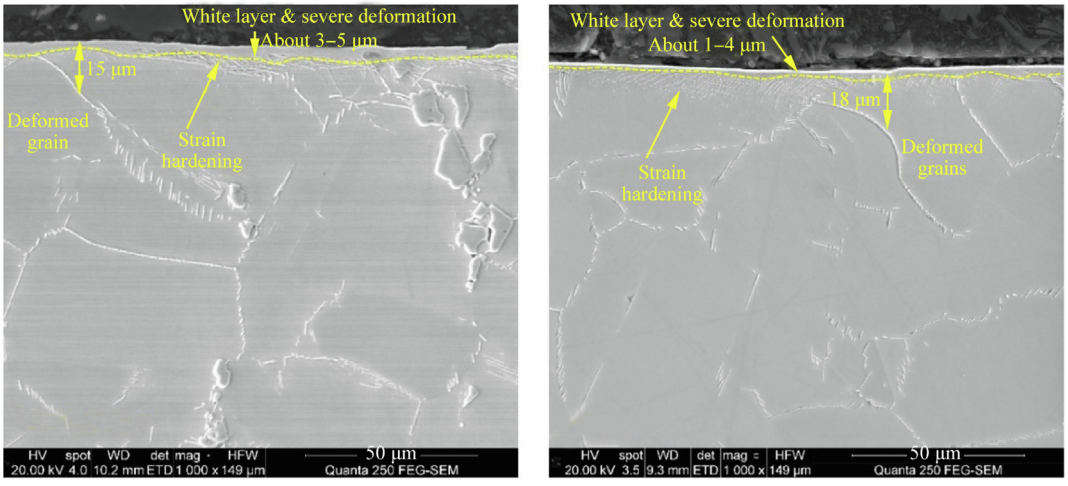

(c) d=4 mm, f=5.0 m/min, s=0.07 mm (d) d=4 mm, f=5.0 m/min, s=0.35 mm

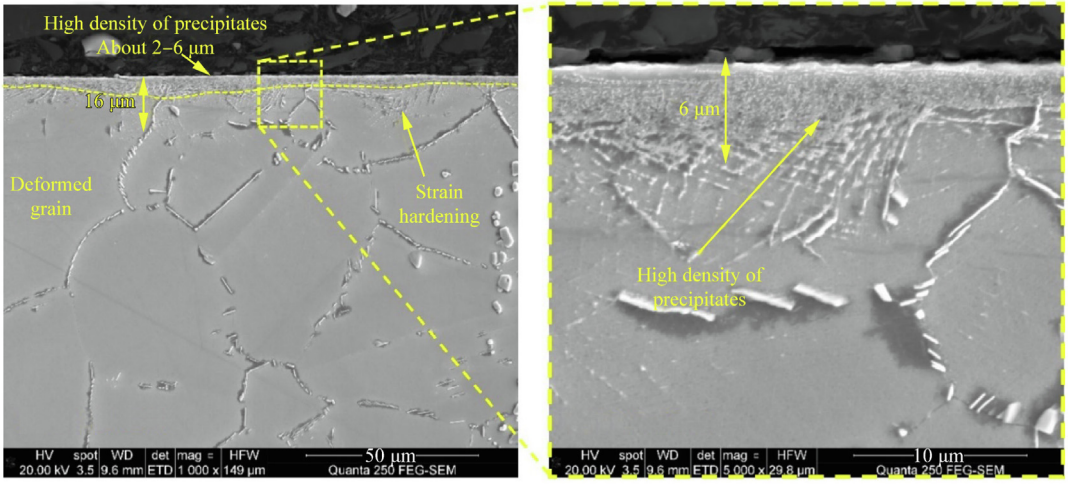

(e) d=4 mm, f=2.5 m/min, s=0.07 mm (f) Enlarged view of Fig. 12(e)

Fig. 12 Microstructure of surface layer affected in stepover direction by hammer peening conditions after thermal exposure at 550 °C.

Table 5 compares the radius a of the circular contact region and the maximum pressure p_0 reached per impact for the selected MHP conditions when impacting with the contact force $P = F_Z$. These were calculated using Eqs. (3)–(6), and F_Z values shown in Fig. 3. The properties of the workpiece material are shown in Table 2. Both indenters were cemented carbide spheres, and although its elastic modulus can vary depending on grain size, we considered an average value of

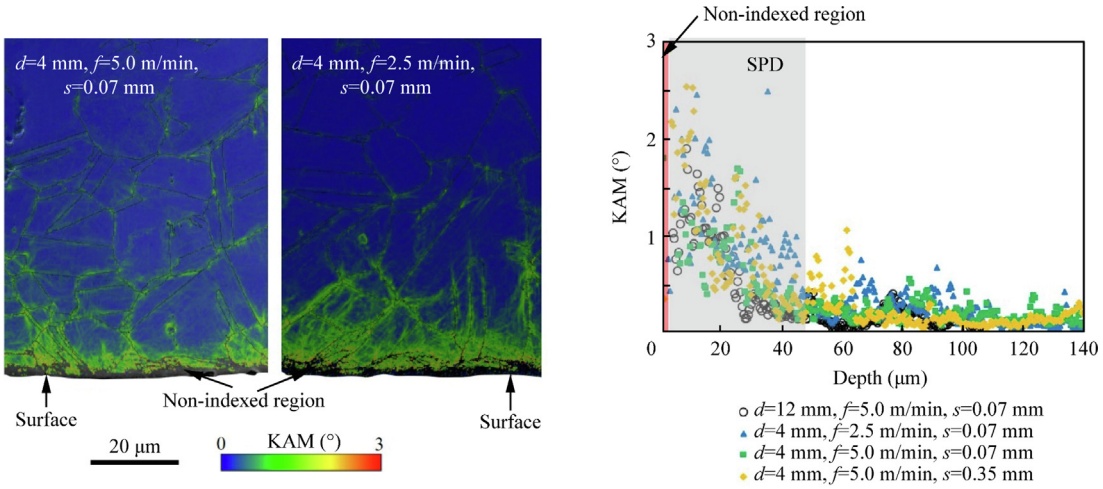

(a) Examples of KAM maps after thermal exposure at 550 ℃ for 20 h

(b) Distribution of KAM across depth after thermal exposure at 550 ℃ for 20 h

Fig. 13 Examples of KAM maps and distribution of KAM across depth within region with maximum deformation of MHP samples after thermal exposure at 550 °C for 20 h.

Table 5 Radius of circular contact region a, maximum pressure p_0 assuming elastic contact, yielding pressure $(p_0)_y$, position of maximum subsurface stress z_{max}, and average surface RS in feed ($\sigma_{RS,\ feed,\ 0}$) and stepover direction ($\sigma_{RS,\ stepover,\ 0}$) of tested MHP conditions.

d (mm)	f (m/min)	s (mm)	a (mm)	p_0 (MPa)	$(p_0)_y$ (MPa)	z_{max} (μm)	$\sigma_{RS,\ feed,\ 0}$ (MPa)	$\sigma_{RS,\ stepover,\ 0}$ (MPa)
12	5.0	0.07	0.38	2 144	1 610	185	–238	–384
4	2.5	0.07	0.27	4 460	1 610	130	–662	–1 435
4	5.0	0.07	0.27	4 541	1 610	127	–642	–1 399
4	5.0	0.35	0.27	4 435	1 610	128	–489	–812

550 GPa from Ref. 41. As expected, the contact region decreased when using the smallest diameter tool, and the maximum pressure p_0 was two times higher than when using the 12 mm diameter tool. As consequence of higher pressure, the thickness of the compressive RS layer increased from about 500 μm when using the 12 mm diameter tool to about 600 when employing the 4 mm diameter tool, independently of the feed rate and stepover value. Under such conditions, the maximum pressure, assuming ideal elastic contact, was higher than the yielding pressure $(p_0)_y$. This confirms, that contact forces induced a misfit of plastic strains from the surface to the bulk, leading to generation of RS to balance the misfit. The classical Hertzian theory predicts the position of the maximum shear stress at depth $z_{max} = 0.48a$.[40] This expression predicts the maximum stress at about 130 μm and 185 μm when using the 4 mm and 12 mm diameter tools respectively. As can be seen in Fig. 6, the presence of a subsurface peak RS is more evident in the feed direction than in the stepover direction since the later accumulated repeated impacts. This subsurface peak is located at about 100 μm depth and therefore closer to the surface. This shift of the peak compressive RS towards the surface is attributed to the sliding motion, which also increases the maximum subsurface von Mises stresses.[39] As can be seen in Table 5, surface RS induced by the 12 mm diameter tool increased by 2.0–3.8 times when using the 4 mm diameter tool. This increase is higher than the increase of contact pressure p_0 even for the same feed rate and stepover distance. This additional increase in the magnitude of compressive RS was possibly caused by the localized friction force generated when sliding the tool across the surface, since sliding also increases von Mises stresses being this effect even more relevant when friction increases.[39]

The RS induced by MHP were determined by the X-ray diffraction method, using a collimator of 1 mm diameter. The distance between successive impacts in the feed direction is $\Delta = f/F$, where F is the hammering frequency, $F = 250$ Hz. Δ is approximately 0.33 mm at feed rate of 5.0 m/min and 0.17 mm at feed rate 2.5 m/min. The circular contact region has a diameter of $2a = 0.54$ mm for the 4 mm diameter tool, and $2a = 0.76$ mm when using the 12 mm diameter tool. Therefore, the contact region of a preceding impact, will be impacted 2–3 times by the successive impacts. Thus, X-ray diffraction measurements determined the average value of RS field induced by several impacts. By contrast, the distance between successive impacts in the stepover direction depends on the stepover distance s. The maximum stepover distance $s = 0.35$ mm was used with the 4 mm diameter tool, and therefore the contact region was impacted 2 times. When reducing the stepover distance to 0.07 mm, the contact region of the 4 mm diameter tool was impacted 7–8 times and 10–11 times the contact region of the 12 mm diameter tool. This analysis demonstrates that for the tested conditions the effect of stepover distance on residual

stresses was relevant because it led to more impacts within the contact region than when reducing the feed. Furthermore, the number of impacts in the stepover direction was also more than in the feed direction, which explains the more compressive surface RS induced in the stepover direction. This finding also suggests that machine hammer peening tools that can work at higher frequency such as piezoelectric actuators could increase the magnitude of surface residual stresses because they can impact more times the same region and at higher velocities.

HP conditions did not alter the near surface microstructure generated by preceding face turning operation. Only a thicker affected layer was identified in the KAM analysis for the surface hammer peened with the 4 mm diameter tool at feed rate 2.5 mm/min and stepover distance 0.07 mm. In fact, this condition used the lowest feed rate and stepover distance, and consequently the surface was impacted more times. Those repeated impacts could possibly produce an accumulation of the deformation beneath the surface. Nevertheless, the analysis of FWHM profiles showed similar behavior in all MHP conditions (see Fig. 9), which means that similar plastic deformation was induced by all tested conditions.

4.2. Linking mechanical properties and surface integrity

This section discusses the link between microstructure and mechanical properties of the MHP surfaces. Fig. 14 compares the microstructure of the surface layer affected by hammer peening with the 12 mm diameter tool at feed rate 5.0 m/min and stepover distance 0.07 mm, and KAM, reduced modulus E_r, hardness H and RS in the stepover direction $\sigma_{RS,\ stepover}$. It should be clarified that this example is representative of all conditions since the effect of process parameters was only relevant in the RS profile.

Three distinctive regions can be observed in Fig. 14. Zone I (< 10–15 μm) consisted of a thin white layer and heavily deformed region, with presence of slip bands and bent grains. This heavily deformed layer was caused by the preceding turning process as discussed in Section 3.4. Fig. 14 shows that the reduced modulus E_r measured by nanohardness, decreased within this region. White layers generated by severe machining conditions in nickel-based alloys are formed by nanocrystals

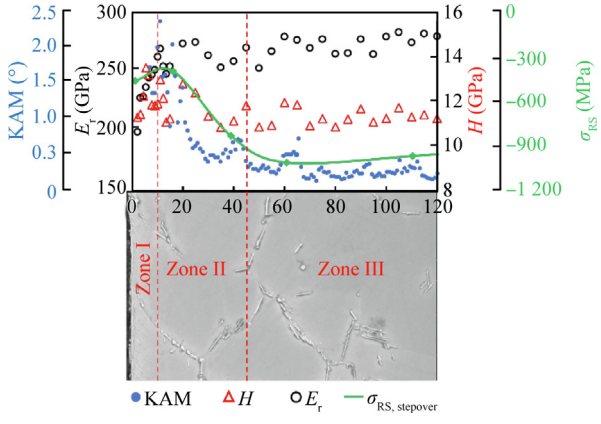

Fig. 14 Microstructure of surface layer affected in stepover direction by hammer peening with d = 12 mm, f = 5.0 m/min, s = 0.07 mm, and KAM, E_r, H and RS profiles of the same condition.

ranging from 20 nm to 100 nm.[38] It is known that elastic modulus for bulk nanocrystalline materials is lower than for conventional coarsely-grained polycrystals,[42] which is consistent with the results of the present study. Liao et al.[43] performed compression tests of nanopillars in a white layer generated in the nickel-based alloy RR1000 and they also found a lower elastic modulus compared to the bulk material. Furthermore, they observed that this behavior was detrimental, since during cyclic loading–unloading tests the white layer accumulated more plastic strain.

Hardness also seems to increase in Zone I, but it is not evident due to the scatter of results. In a recent work, Ding et al.[44] also conducted nanohardness measurements in severely deformed machined layers with the presence of white layers and they found an increase in hardness. Furthermore, it is widely accepted that a reduction of grain size increases the FWHM.[45] Although not included in Fig. 14 to avoid overwriting, FWHM profiles showed the highest values within Zone I (see Fig. 9), which is the contribution of the reduced size of the grains and high degree of work-hardening. The microstructure and most of the mechanical properties of Zone I were affected by the preceding turning process, but importantly, selected MHP processes showed the ability to induce compressive RS which varied depending on the selected conditions (see Fig. 6).

The secondary electron images taken in the SEM did not show evidence of severe deformation in Zone II (from about 10 μm to about 50 μm depth) as can be observed in Fig. 14. Accordingly, the reduced modulus E_r was similar to the bulk material. However, the KAM significantly increased, as consequence of the dislocations induced by turning and subsequent MHP. FWHM profiles also showed the same trend (see Fig. 9). This explains the work-hardening experienced by the material within this region, since H increases 10%–15% with respect to the bulk value. RS also significantly changed within this transition layer. In fact, elastic RS are generated to balance the misfit of plastic strains. In Zone II, the steep gradient of KAM and FWHM suggests the plastic strain decreasing from the surface to the bulk, and therefore significant changes in RS are plausible.

Zone III extends from about 50 μm to about 500 μm depth where bulk properties are reached (note that Fig. 14 was limited to 120 μm to appropriately visualize the characteristics of Zones I and II). This is the less affected region since microstructural defects are not found, and E_r, H and KAM values remain constant. However, there is a presence of compressive RS which gradually decrease their value to finally stabilize at bulk values (see Fig. 6). The variations of RS up to 400 μm depth were low since low values of KAM and FWHM also suggest low plastic strain misfit.

4.3. Effect of temperature on surface integrity and mechanical properties

In-situ annealing tests allowed us to track the evolution of surface RS during heating and isothermal exposure at 550 °C. The RS relaxation kinetics changes over time because the superalloy experiences both microstructure and crystal structure changes,[28] and the relaxation process can be divided into different stages. It is widely accepted that RS induced by heat treatments,[26,27] peening processes[19] or machining[46] in nickel-based alloys mostly relax in two stages: (A) Rapid relaxation

of RS during heating up or early stage of the exposure (Stage I) and (B) Lower relaxation during isothermal exposure as consequence of creep mechanism (Stage II). This has also been observed in recent *in-situ* neutron diffraction experiments to study the relaxation of residual stresses in welded steel components.[22–25]

Fig. 15(a) shows surface RS of the selected MHP conditions at the initial state ($\sigma_{RS,\ initial}$), during heating up at 300 °C ($\sigma_{RS,\ 300\ °C}$), when reaching 550 °C ($\sigma_{RS,\ 550\ °C}$) and after the isothermal exposure of 20 h ($\sigma_{RS,\ final}$). The surface treated with the 4 mm diameter tool at feed rate 2.5 m/min and stepover 0.07 mm was measured in the feed direction due to an incorrect orientation of the specimen in the *in-situ* annealing test. For the best of the authors knowledge, this is the first time that peening-induced surface RS have been measured *in-situ* during heating up period. *In-situ* neutron experiments have found relaxation of tensile residual strains from the beginning of the heating exposure.[22–25] However, the heating up period was divided into two stages. At the beginning of exposure up to 300 °C (Stage I-a), surface RS became even more compressive. This might be associated with the experimental set-up used in the laboratory X-ray diffraction measurements. During heating up, the temperature is not homogenous in the sample. The regions closer to the heating source and center of the sample are hotter than the external regions. Consequently, the center region tries to expand, but the outer region restricts this deformation, leading to an increase of compressive RS in the central region (note that surface RS were measured at the center of the specimen). Thermal relaxation of RS occurred from 300 °C to 550 °C (Stage I-b), which is probably due to creep relaxation[22–27] and annihilation of dislocations. The magnitude of increase of compressive RS (Stage I-a) and subsequent relaxation (Stage I-b) was similar in all cases, independently of the initial RS state.

The relaxation of RS during isothermal exposure (Stage II) is dominated by thermally activated process or creep mechanism.[19,22–27] The relaxation of RS was almost negligible at the starting of the isothermal exposure if $\sigma_{RS,\ 550\ °C}$ was less compressive than –450 MPa. However, the highest compressive RS (–877 MPa) exhibited a significant relaxation. Despite the high relaxation, this MHP conditions still had the highest compressive RS after cooling down. This confirms that the relaxation during isothermal exposure also depends on the magnitude of the RS at the beginning of this process.[46] Importantly, all hammer peened surfaces kept surface compressive RS after the thermal treatment. It should be clarified that we tested the residual stress relaxation at 550 °C because this was the in-service temperature established by the aero-engine manufacturer that we collaborate with. However, Inconel 718 is used up to 650 °C in some applications, and a further significant relaxation of residual stresses (60%–70%) is expected at that temperature, even at short exposure periods as reported in studies conducted with shot-peened samples.[18,19]

As explained in Section 3.6, no significant changes were observed in the microstructure after thermal exposure and mechanical properties. To further analyze the effect of thermal exposure on the surface layer properties, the FWHM measured at the initial state and after the thermal exposure were compared. As can be seen in Fig. 15(b), FWHM reduced about 20% in all surface conditions as consequence of the annihilation of dislocations, and therefore a reduction of the work-hardening.

5. Conclusions

This work has studied the use of small diameter tools to improve the surface integrity of nickel-based alloy components

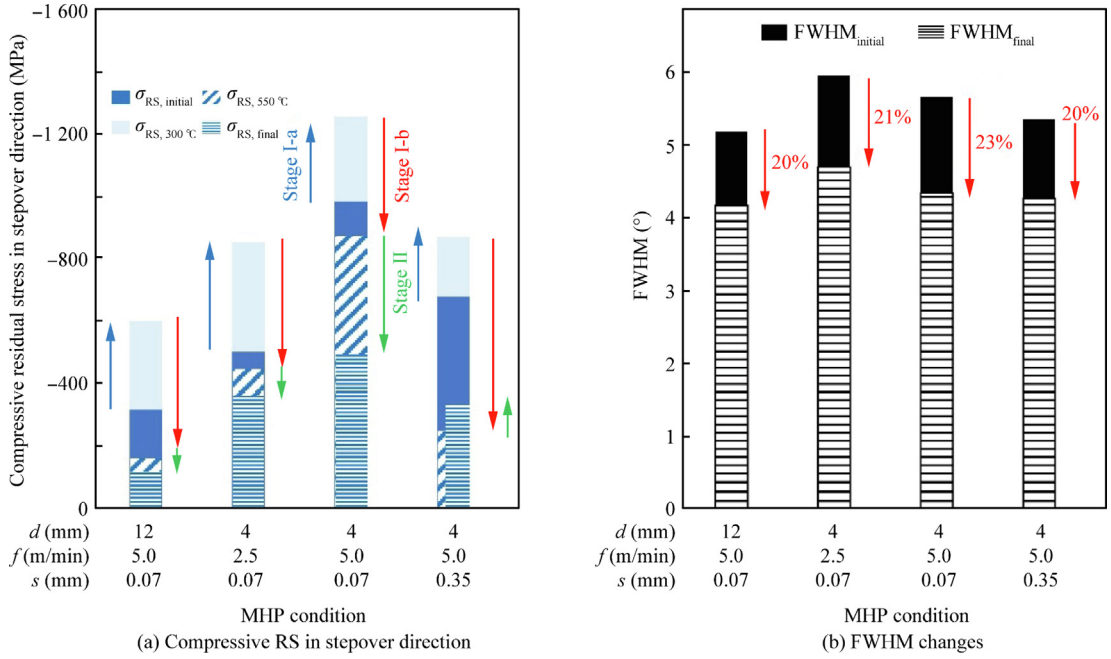

Fig. 15 Compressive RS in stepover direction and FWHM changes during *in-situ* annealing tests.

by MHP. Additionally, *in-situ* annealing tests combined with X-ray diffraction measurements were conducted to analyze the stability of compressive RS induced by MHP. The key conclusions are:

(1) The study demonstrates that MHP with small diameter tools (4 mm) significantly improves the SI generated by preceding machining operation, and reference SP and LSP treatments. The best condition (5.0 m/min feed rate and 0.07 mm stepover distance) can generate compressive RS above –1 000 MPa in both directions and a thick compressive layer (0.5–0.6 mm), as well as a homogenous smooth surface (Ra < 0.8 μm in the feed and stepover direction). This improvement in SI is fundamentally consequence of (A) The high contact pressure reached when reducing the diameter of the tool, and (B) More repeated impacts when reducing the stepover distance. Despite the high pressures and friction forces caused during sliding, the microstructure of the MHP surfaces was not adversely affected with respect to the as-machined condition.

(2) The relationship between the microstructure and mechanical properties of the MHP surfaces can be divided into three zones. Zone I (< 10–15 μm) was formed by a thin white layer and heavily deformed region caused by the preceding turning process. These alterations led to a reduced modulus E_r, increased hardness H, and FWHM values. This finding remarks the need to avoid surface damage in the last machining operation. Interestingly, selected MHP processes induced high compressive RS which could counterbalance the altered microstructure. Zone II (from about 10 μm to about 50 μm depth) did not show an altered microstructure, and consequently the reduced modulus E_r was similar to the bulk material. However, the KAM and FWHM significantly increased, as consequence of the work-hardening experienced by the material within this region. This was also evidenced by 10%–15% hardness increase in most cases with respect to the bulk value. RS also significantly changed within this transition layer to balance the misfit of plastic strains which is significant as suggested by the steep gradient of KAM and FWHM profiles. Finally, Zone III extends from about 50 μm to about 500 μm, and there is absence of microstructural defects, and E_r, H and KAM values remained constant at bulk values. Importantly, there was presence of compressive RS which gradually decrease to finally stabilize at bulk values.

(3) *In-situ* annealing tests combined with X-ray diffraction measurements showed that heating up process can be divided into two stages: (A) At the early-stage additional compressive stresses are generated because the expansion of the central region is restricted by the outer region that it is at lower temperature; (B) Above 300 °C, compressive RS start relaxing as a consequence of annihilation of dislocations and creep mechanism. Isothermal exposure at 550 °C also caused additional relaxation, being this relaxation higher when the initial magnitude of RS was higher. Importantly, compressive RS induced by MHP remained compressive after the long thermal exposure.

CRediT authorship contribution statement

Aitor MADARIAGA: Writing – original draft, Methodology, Investigation, Formal analysis, Conceptualization. **Gorka ORTIZ-DE-ZARATE:** Writing – review & editing, Methodology, Investigation, Conceptualization. **Pedro José ARRAZOLA:** Writing – review & editing, Resources, Funding acquisition.

Declaration of competing interest

The authors declare that they have no known competing financial interests or personal relationships that could have appeared to influence the work reported in this paper.

Acknowledgements

The authors thanked the financial support given by EPSRC to the Grant LOFAMO (No. EP/X023281/1), as well as the Basque Government for the financial support given from Elkartek Program to the Project FRONTIERS 2022—Superficies Multifuncionales en la Frontera del Conocimiento (No. KK-2022/00109). The authors acknowledged Denis SORIANO for the assistance in the turning and machine hammer peening tests, and the Electron Microscopy Facility, the X-ray Diffraction Laboratory and Nanomechanical Characterisation Laboratory in the Department of Materials of the University of Manchester.

References

1. Cui X, Li CH, Ding WF, et al. Minimum quantity lubrication machining of aeronautical materials using carbon group nanolubricant: From mechanisms to application. *Chin J Aeronaut* 2022;**35**(11):85–112.
2. Ezugwu EO. High speed machining of aero-engine alloys. *J Braz Soc Mech Sci & Eng* 2004;**26**(1):1–11.
3. Jawahir IS, Brinksmeier E, M'Saoubi R, et al. Surface integrity in material removal processes: Recent advances. *CIRP Ann* 2011;**60**(2):603–26.
4. Teti R, Jemielniak K, O'Donnell G, et al. Advanced monitoring of machining operations. *CIRP Ann* 2010;**59**(2):717–39.
5. Ulutan D, Ozel T. Machining induced surface integrity in titanium and nickel alloys: A review. *Int J Mach Tools Manuf* 2011;**51**(3):250–80.
6. Thakur A, Gangopadhyay S. State-of-the-art in surface integrity in machining of nickel-based super alloys. *Int J Mach Tools Manuf* 2016;**100**:25–54.
7. Jin SY, Liu Q, Zhu Y, et al. Surface smoothening and strengthening combined effect of mechanical hammer peening on inconel 718 superalloy. *Mater Manuf Process* 2023;**38**(10):1331–7.
8. Klotz T, Delbergue D, Bocher P, et al. Surface characteristics and fatigue behavior of shot peened Inconel 718. *Int J Fatigue* 2018;**110**:10–21.
9. Kattoura M, Mannava SR, Qian D, et al. Effect of laser shock peening on residual stress, microstructure and fatigue behavior of ATI 718Plus alloy. *Int J Fatigue* 2017;**102**:121–34.
10. Chan WL, Cheng HKF. Hammer peening technology—The past, present, and future. *Int J Adv Manuf Technol* 2022;**118**(3):683–701.

11. Schulze V, Bleicher F, Groche P, et al. Surface modification by machine hammer peening and burnishing. *CIRP Ann* 2016;**65**(2):809–32.
12. Bleicher F, Lechner C, Habersohn C, et al. Mechanism of surface modification using machine hammer peening technology. *CIRP Ann* 2012;**61**(1):375–8.
13. Chen T, John H, Xu J, et al. Influence of surface modifications on pitting corrosion behavior of nickel-base alloy 718. Part 1: effect of machine hammer peening. *Corros Sci* 2013;**77**:230–45.
14. Chen T, John H, Xu J, et al. Influence of surface modifications on pitting corrosion behavior of nickel-base alloy 718. Part 2: effect of aging treatment. *Corros Sci* 2014;**78**:151–61.
15. Trauth D, Klocke F, Welling D, et al. Investigation of the surface integrity and fatigue strength of Inconel718 after wire EDM and machine hammer peening. *Int J Mater Form* 2016;**9**(5):635–51.
16. Klocke F, Trauth D, Schongen F, et al. Time-efficient process design for tapping: prediction of the surface layer condition using similarity mechanics. *Wt Online* 2013;**103**(10):758–63 [German].
17. Sarasua Miranda JA, Cristobal AT, González-Barrio H, et al. Comparative study of finishing techniques for age-hardened Inconel 718 alloy. *J Mater Res Technol* 2021;**15**:5623–34.
18. Khadhraoui M, Cao W, Castex L, et al. Experimental investigations and modelling of relaxation behaviour of shot peening residual stresses at high temperature for nickel base superalloys. *Mater Sci Technol* 1997;**13**(4):360–7.
19. Prevey PS, Hombach DJ, Mason PW. Thermal residual stress relaxation and distortion in surface enhanced gas turbine engine components. *17th ASM heat treating society conference*. Materials Park: Heat Treating Society; 1997. p. 3–12.
20. Foss BJ, Gray S, Hardy MC, et al. Analysis of shot-peening and residual stress relaxation in the nickel-based superalloy RR1000. *Acta Mater* 2013;**61**(7):2548–59.
21. Li YG, Geng JW, Wang ZP, et al. Thermal evolutions of residual stress and strain hardening of GH4169 Ni-based superalloy treated by laser shock peening. *Surf Coat Technol* 2023;**467**:129690.
22. Chen B, Skouras A, Wang YQ, et al. *In situ* neutron diffraction measurement of residual stress relaxation in a welded steel pipe during heat treatment. *Mater Sci Eng A* 2014;**590**:374–83.
23. Dodge MF, Gittos MF, Dong H, et al. *In-situ* neutron diffraction measurement of stress redistribution in a dissimilar joint during heat treatment. *Mater Sci Eng A* 2015;**627**:161–70.
24. Alipooramirabad H, Paradowska A, Lavigne O, et al. *In situ* neutron diffraction measurement of strain relaxation in welds during heat treatment. *Sci Technol Weld Join* 2017;**22**(6):484–95.
25. Alipooramirabad H, Paradowska A, Reid M, et al. Effect of holding time on strain relaxation in high-strength low-alloy steel welds: an *in situ* neutron diffraction approach. *J Manuf Process* 2022;**73**:326–39.
26. Rolph J, Evans A, Paradowska A, et al. Stress relaxation through ageing heat treatment–a comparison between *in situ* and *ex situ* neutron diffraction techniques. *Comptes Rendus Phys* 2012;**13**(3):307–15.
27. Aba-Perea PE, Pirling T, Preuss M. *In-situ* residual stress analysis during annealing treatments using neutron diffraction in combination with a novel furnace design. *Mater Des* 2016;**110**:925–31.
28. Chen Y, Cernatescu I, Venkatesh V, et al. On the residual stress relaxation in Inconel 718 superalloys at high temperature by real-time neutron diffraction. *Mater Des* 2023;**232**:112135.
29. Cao Y, Zhu YJ, Ding WF, et al. Vibration coupling effects and machining behavior of ultrasonic vibration plate device for creep-feed grinding of Inconel 718 nickel-based superalloy. *Chin J Aeronaut* 2022;**35**(2):332–45.
30. Chaabani S, Arrazola PJ, Ayed Y, et al. Comparison between cryogenic coolants effect on tool wear and surface integrity in finishing turning of Inconel 718. *J Mater Process Technol* 2020;**285**:116780.
31. Oliver WC, Pharr GM. Measurement of hardness and elastic modulus by instrumented indentation: Advances in understanding and refinements to methodology. *J Mater Res* 2004;**19**(1):3–20.
32. Aba-Perea PE, Pirling T, Withers PJ, et al. Determination of the high temperature elastic properties and diffraction elastic constants of Ni-base superalloys. *Mater Des* 2016;**89**:856–63.
33. Madariaga A, Cuesta M, Dominguez E, et al. Enhancing surface integrity of A7050-T7451 aluminium alloy by pneumatic machine hammer peening. *Procedia CIRP* 2022;**108**:317–22.
34. Madariaga A, Cuesta M, Ortiz-de-Zarate G, et al. Correcting distortions of thin-walled machined parts by machine hammer peening. *Chin J Aeronaut* 2024;**37**(6):439–53.
35. Kwong J, Axinte DA, Withers PJ. The sensitivity of Ni-based superalloy to hole making operations: influence of process parameters on subsurface damage and residual stress. *J Mater Process Technol* 2009;**209**(8):3968–77.
36. Naskar A, Paul S. Non-destructive measurement of grinding-induced deformation-depth using grazing incidence X-ray diffraction technique. *NDT E Int* 2022;**126**:102592.
37. Madariaga A, Esnaola JA, Fernandez E, et al. Analysis of residual stress and work-hardened profiles on Inconel 718 when face turning with large-nose radius tools. *Int J Adv Manuf Technol* 2014;**71**(9):1587–98.
38. M'Saoubi R, Axinte D, Herbert C, et al. Surface integrity of nickel-based alloys subjected to severe plastic deformation by abusive drilling. *CIRP Ann* 2014;**63**(1):61–4.
39. Ali F. Numerical study on subsurface stress in Hertzian contacts under pure sliding conditions. *J Appl Comput Mech* 2020;**6**(SI):1098–106.
40. Bhushan B. Introduction to tribology. *Contact between solid surfaces*. New York: John Wiley & Sons Ltd; 2013. p. 91–155.
41. Herd S. Development of a new approach for modelling the tribocorrosion of cemented tungsten carbide in oil and gas drilling environments [dissertation]. Southampton: University of Southampton; 2017.
42. Kim TY, Dolbow JE, Fried E. Numerical study of the grain-size dependent Young's modulus and Poisson's ratio of bulk nanocrystalline materials. *Int J Solids Struct* 2012;**49**(26):3942–52.
43. Liao ZR, Polyakov M, Diaz OG, et al. Grain refinement mechanism of nickel-based superalloy by severe plastic deformation—Mechanical machining case. *Acta Mater* 2019;**180**:2–14.
44. Ding RG, Knaggs C, Li HY, et al. Characterization of plastic deformation induced by machining in a Ni-based superalloy. *Mater Sci Eng A* 2020;**778**:139104.
45. Unal O, Varol R. Surface severe plastic deformation of AISI 304 *via* conventional shot peening, severe shot peening and repeening. *Appl Surf Sci* 2015;**351**:289–95.
46. Madariaga A, Aperribay J, Arrazola PJ, et al. Effect of thermal annealing on machining-induced residual stresses in Inconel 718. *J Mater Eng Perform* 2017;**26**(8):3728–38.